BOLETIN DE LA SOCIEDAD ESPAÑOLA DE
Cerámica y Vidrio
www.elsevier.es/bsecv

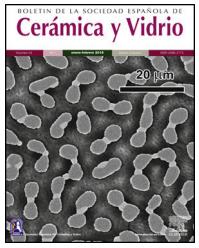

Original

Preparation of lithium iron phosphate composites by electrodeposition with a tunnel structure on aluminium foil surface

*Xiaolong Liang, Rengui Xiao, Xia Liao**

Escuela de Química e Ingeniería Química, Universidad de Guizhou, Guiyang 550003, China

ARTICLE INFO

Article history:
Received 31 July 2019
Accepted 4 December 2019
Available online 10 January 2020

Keywords:
Tunnel hole
Aluminium foil current collector
Propylene carbonate
Electrodeposition
Lithium iron phosphate
Polyanion

ABSTRACT

In this paper, aluminium foil with a tunnel structure was used as a cathode to prepare a lithium iron phosphate composite by electrochemical deposition using propylene carbonate as the electrolyte solvent, and lithium nitrate, ferric nitrate and phosphoric acid as raw materials. The results show that the positive electrode composite is composed of a mixture of an olivine structured $LiFePO_4$ and polyanion $Li_9Al_3P_8O_{29}$. The chemical composition of the mixture is related to the voltage of the electrochemical deposition and the acidity of the electrolyte solution. For a voltage of 1.8 V and pH of 1.0, the composite material deposited in the tunnel of the aluminium foil takes the form of a one-dimensional nanotube, with a particle size ranging from 80 nm to100 nm. The composite material is closely combined with the aluminium foil. The aluminium foil can be directly used as a positive current collector, with a lithium sheet as the negative electrode. After mounting into a battery, an electrochemical performance test is performed. The battery test results show an initial discharge capacity of 95 mAh/g, 79 mAh/g and 59 mAh/g at 0.1 C, 0.2 C and 0.5 C, respectively. After the material is doped with magnesium and cobalt, the initial discharge capacity of the battery is 100 mAh/g and 130 mAh/g, respectively, at a rate of 0.1 C. The cyclic voltammetry analysis of the battery show that after electrochemical deposition of the element, the symmetry between the oxidation and reduction peaks is increased, and the difference between the oxidation and reduction peak potentials is reduced. Element doping improves battery cycle performance. The AC impedance analysis show that the embedding impedance for lithium ions at the SEI interface is reduced from 300 Ω to 250 Ω, 100 Ω after doping with magnesium, and cobalt. And the reaction mechanism of electrochemical deposition is discussed.

© 2019 Published by Elsevier España, S.L.U. on behalf of SECV. This is an open access article under the CC BY-NC-ND license (http://creativecommons.org/licenses/by-nc-nd/4.0/).

* *Corresponding author.*
E-mail address: xliao@gzu.edu.cn (X. Liao).
https://doi.org/10.1016/j.bsecv.2019.12.003
0366-3175/© 2019 Published by Elsevier España, S.L.U. on behalf of SECV. This is an open access article under the CC BY-NC-ND license (http://creativecommons.org/licenses/by-nc-nd/4.0/).

Preparación de compuestos de matriz de aluminio de fosfato de hierro y litio por deposición electroquímica

Palabras clave:
Agujero del túnel
Colector de corriente de papel de aluminio
Carbonato de propileno
Electrodeposición
Fosfato de litio y hierro
Polianión

R E S U M E N

En este trabajo se usó papel de aluminio con una estructura de poro túnel como cátodo para preparar un compuesto de matriz de aluminio de fosfato de hierro y litio por deposición electroquímica usando carbonato de propileno como disolvente electrolítico, y nitrato de litio, nitrato férrico y ácido fosfórico como materias primas. Los resultados muestran que el compuesto de electrodo positivo está compuesto por una mezcla de $LiFePO_4$ estructurado de olivino y polianión $Li_9Al_3P_8O_{29}$. La composición química de la mezcla está relacionada con el voltaje de la deposición electroquímica y la acidez de la solución electrolítica. Para un voltaje de 1,8 V y un pH de 1,0, el material compuesto depositado en el agujero del túnel del papel de aluminio toma la forma de un nanotubo unidimensional, con un tamaño de partícula que varía de 80-100 nm. El material compuesto se combina estrechamente con el papel de aluminio. El papel de aluminio se puede usar directamente como un colector de corriente positiva, con una lámina de litio como electrodo negativo. Después de montar en una batería, se realizó una prueba de rendimiento electroquímico. Los resultados de la prueba de batería muestran una capacidad de descarga inicial de 95, 79 y 59 mAh/g en condiciones de 0,1, 0,2 y 0,5 °C, respectivamente. Después de dopar el material con magnesio y cobalto, la capacidad de descarga inicial de la batería fue de 100 y 130 mAh/g, respectivamente, a una velocidad de 0,1 °C. Los resultados del análisis de voltamperometría cíclica de la batería muestran que después de la electroquímica Deposición del elemento, se aumenta la simetría entre los picos de oxidación y reducción, y se reduce la diferencia entre los potenciales de pico de oxidación y reducción. El dopaje de elementos mejora el rendimiento del ciclo de la batería. Los resultados del análisis de impedancia de CA muestran que la impedancia de incrustación para iones de litio en la interfaz SEI se reduce de 300 a 250 y 100 Ω después de dopaje con magnesio y cobalto. Este artículo analiza y discute el mecanismo de reacción para los compuestos de deposición electroquímica.

© 2019 Publicado por Elsevier España, S.L.U. en nombre de SECV. Este es un artículo Open Access bajo la licencia CC BY-NC-ND (http://creativecommons.org/licenses/by-nc-nd/4.0/).

Introduction

The lithium-ion battery cathode material $LiFePO_4$ [1,2] has a low preparation cost, good cycle performance, high safety and stability, and offers environmental protection and non-toxicity, with a theoretical capacity of 170 mAh/g. As a widely used clean energy carrier, the most commonly used preparation methods are the solid phase method [3,4], hydrothermal method [5,6], microwave method [7,8], etc. To improve the performance of $LiFePO_4$ materials, various modification methods such as doping, nanocrystallization and carbon coating are commonly used. The electrochemical properties of the material can also be improved by controlling the topography of the material. Zhou Y et al. developed a hollow spherical lithium iron phosphate [9–11], which shortened the lithium-ion migration path, reduced the resistance to lithium-ion migration, and improved the material properties. Electrochemical deposition methods have been studied in the preparation of transition metal oxides (LTMOs) for lithium-ion battery materials [12–14]. Zhen Quan [15] et al. electrodeposited a manganese oxide precursor onto an anode gold foil by electrochemical deposition. Then, the surface of the precursor film was immersed into a 0.03 mol/L LiOH solution and sintered at a high temperature to obtain a nanocrystalline $LiMn_2O_4$ film material. The material showed good cycle performance and stability. Huigang Zhang [16] et al. proposed the preparation of $LiCoO_2$ and $LiMn_2O_4$ cathode materials for lithium-ion batteries by direct electrodeposition under high temperature using a molten salt as electrolyte under argon-protected sealed conditions. A mesoporous foamed carbon was used as a deposit carrier working electrode during the electrodeposition process, and a pulse voltage was applied. The prepared material was superimposed into a one-dimensional nanowire structure in a sheet form. The results show that the prepared samples have good performance in terms of crystallinity and electrochemical capacity performance. In summary, during the electrochemical deposition process, the structure of the working electrode plays a role in the template preparation process. Electrodeposition improves the morphology and electrochemical performance of the material.

However, the electrodeposition preparation method has not been reported in the preparation of lithium iron phosphate materials. In this paper, we used an organic solvent as the electrolyte and a high-purity aluminium foil [17] with a tunnel structure as the negative electrode material. At room temperature, a lithium iron phosphate material having nano size holes in the tunnel structure was prepared by way of electrodeposition. We studied the reaction mechanism in the electrodeposition process and tested the electrochemical properties of the composite materials. At the same time, the characteristics of lithium-ion battery current collectors

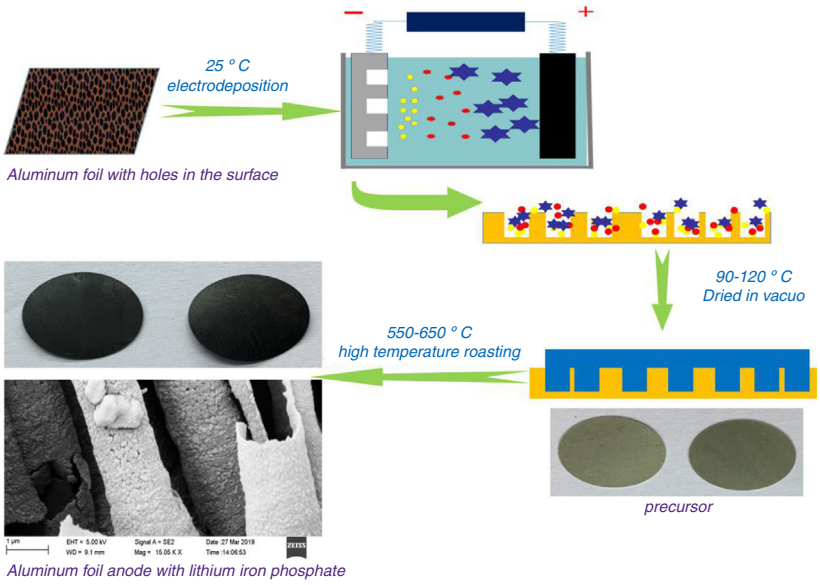

Fig. 1 – Schematic diagram of electrochemical deposition of positive electrode composite materials for lithium-ion batteries.

for aluminium foil with a tunnel structure are studied. This study presents a useful exploration for reducing the interface resistance between the current collector and the electrode material.

Experimental

Preparation of materials

The electrolyte used in the electrodeposition process was organic propylene carbonate as a solvent. Ferric nitrate, lithium nitrate, and phosphoric acid were added while maintaining a phosphorus:iron:lithium molar ratio of 1:0.3:1. After thoroughly stirring and dissolving, 0.03 mol/L of glucose and 0.005 mol/L of cationic surfactant cetyltrimethylammonium bromide were added. At 25 °C, aluminium foil with a thickness of 110 μm was used as the cathode. The surface of the aluminium foil contained a large number of square tunnel pore structures with an inner diameter of approximately 1 μm. An equal-area graphite plate is used as the anode, and the distance between the two plates is maintained at 0.4–1.0 cm. The graphite plate was used as an anode and electrochemically deposited onto the surface of the cathode aluminium foil under a constant voltage of 1.8 V DC. A lithium iron phosphate precursor was prepared. The precursor material was vacuum dried at 90–120 °C for 3–6 h and then calcined at 550–650 °C for 5–8 h under nitrogen protection. An aluminium-based positive electrode composite material having a surface-containing lithium iron phosphate conductive active material was obtained. Different transition metal salts such as magnesium nitrate and cobalt nitrate were added to the organic electrolyte to perform metal-ion doping modification. Fig. 1 shows a schematic view of the process preparing a lithium iron phosphate composite by electrochemical deposition.

Characterization of materials

The crystal structure of the composite was characterized by an X'PERT PRO X-ray diffractometer (XDR) produced by PANalytical B. V., the Netherlands. A $\sum$IGMA type field-emission scanning electron microscope (SEM) was used to characterize the morphology of the composite material. The composite material was subjected to XPS (American Thermo Fisher) characterization and the elemental valence state was studied. Thermogravimetric analysis of the composite precursor was carried out using a model STA 2500 thermogravimetric analyzer manufactured by Netzsch, Germany.

Characterization of electrochemical performance

With lithium as the negative electrode, Celgard 2400 as the diaphragm, and 1 mol/L Li PF_6/EC + DEC (volume ratio of 1:1) as the electrolyte, a CR2032 button battery was assembled in a vacuum glove box filled with argon. A LAND battery test system from the Wuhan Blue Electric Electronics Co., LTD. was used for battery charge and discharge testing. AC impedance test and cyclic voltammetry tests were carried out using an electrochemical workstation manufactured by Shanghai Chenhua Instrument Co., Ltd.

Results and discussion

Phase analysis and characterization

Fig. 2 shows the diffraction pattern of an electrochemical deposited composite material. The XRD pattern of the prepared sample was compared with the standard cards for olivine-type lithium iron phosphate (JCPDScard No. 40-1499) and the polyanion positive electrode material $Li_9Al_3P_8O_{29}$ (JCPDScard No. 52-1463). The results show that the composite cathode material mainly contains an olivine structured

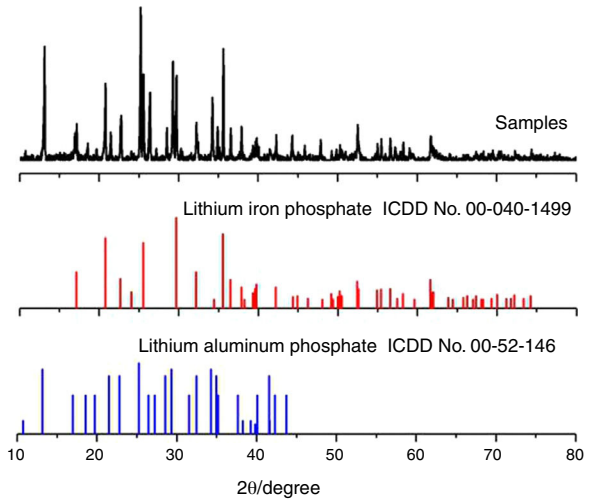

Fig. 2 – XRD analysis of the composites compared with $LiFePO_4$ standard cards and compared with $Li_9Al_3P_8O_{29}$ standard cards.

lithium iron phosphate and polyanion cathode material $Li_9Al_3P_8O_{29}$. As shown in Fig. 1, lithium iron phosphate is mainly produced by an electrochemical reaction process. However, the polyanionic anode material $Li_9Al_3P_8O_{29}$ is produced by corrosion and dissolution of aluminium foil in the cathodic reaction process, which is obtained in the subsequent high-temperature heating process.

In the electrochemical synthesis reaction process shown in Fig. 1, the pH value for the acid electrolyte ranges from 1.0 to 1.2. The aluminium foil is used as a cathode, and the Li^+, Fe^{3+}, and H^+ cations in the electrolyte migrate to the cathode aluminium foil under the action of the cathode potential. At the same time, a corresponding reduction reaction (1) and (2) occurs on the aluminium foil. In this way, the electromigrated Li^+ to the cathode and the reduced Fe^{2+} formed the essential components of the lithium iron phosphate. Meanwhile, in the initial stage of strong acidity, the dissolution reaction of the aluminium oxide film (3) occurs first on the surface of the aluminium foil (an approximately 50 nm thick alumina film will be formed on the surface of the aluminium foil in the natural state). After the removal of the oxide film, the corrosion reaction of aluminium metal occurs under acidic conditions (4). As a competitive reaction within the whole cathodic electrochemical process, the obtained Al^{3+} enters the precursor and is converted into the polyanionic cathode material $Li_9Al_3P_8O_{29}$ during subsequent heating reaction.

The reactions of the cathode are as follows:

$$Fe^{3+} + e^- \rightarrow Fe^{2+} \quad (1)$$

$$2H^+ + 2e^- \rightarrow H_2\uparrow \quad (2)$$

$$Al_2O_3 + 6H^+ \rightarrow 2Al^{3+} + 3H_2O \quad (3)$$

$$2Al + 6H^+ \rightarrow 2Al^{3+} + 3H_2 \quad (4)$$

The reduction reaction (5) and (6) of NO_3^- containing an oxygen radical near the cathode results in the formation of an alkaline gradient around the cathode, thus resulting in deprotonation and dehydrogenation of propylene carbonate (PC) (7). Lithium ions in solution combine with PC^- to produce organic lithium salts on the surface of the aluminium foil cathode (8). The metal cations obtained by reaction (1) and (3) and (4) react with PO_4^{3-} to form the corresponding phosphates, respectively. The precursors for the preparation of the composite materials were composed of the products obtained by reaction (8)–(10) and the mixture of organic propylene carbonate.

$$NO_3^- + 4e^- + 2H^+ \rightarrow NO_2^- + H_2O \quad (5)$$

$$NO_2^- + 3H_2O \rightarrow NO_3^- + 2OH^- + 2H_2\uparrow \quad (6)$$

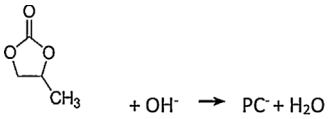

(7)

$$PC^- + Li^+ \rightarrow PC\text{-}Li \quad (8)$$

$$Fe^{2+} + PO_4^{3-} \rightarrow Fe_3(PO_4)_2 \quad (9)$$

$$Al^{3+} + PO_4^{3-} \rightarrow AlPO_4 \quad (10)$$

Fig. 3 shows a scanning electron microscopic view of the composite material. Fig. 3A shows the surface morphology of the composites. The results show that the surface composites are spherical particles with sizes in the range of 100–200 nm and that the particles are interconnected by a network of carbon. Fig. 3B shows the morphology and structure of the composite material in the tunnel holes of the aluminium foil. The results show that the composite material is deposited in the tunnel walls of the aluminium foil. Fig. 3C and D shows enlarged diagrams for the tunnel structure. The results show that the particle size of composite material in the tunnel is about 80–100 nm. The composite material grows along the inner wall of the tunnel with a hollow structure. The tube wall is a one-dimensional nanotube with a thickness of approximately 100 nm. The composite material is closely combined with the wall of the tunnel hole. This embedded structure enlarges the connection between the battery active material and collector fluid. The contact area is conducive to reducing the interface resistance, which increases the electronic conductivity.

XPS elemental analysis for the composites is shown in Fig. 4. Fig. 4A shows the XPS carbon element analysis. The C1 binding energy is 284.8 eV, corresponding to the carbon element; C2 is the calibration peak,is the adventitious carbon; C3 has a binding energy of 288 eV, corresponding to the C=O bond. This shows that in lithium iron phosphate, some carbon exists in the form of carbonaceous compounds. The results show that the carbon element in composites mainly encapsulates electrically active materials in the form of an elementary substance, which plays an important role in the conductivity of the materials. However, some of the carbon still exists in the form of compounds, which affects the electrochemical properties of the materials. How to control the carbon content in the carbon coating needs to be further explored. Fig. 4B shows the analysis of the Fe element in composite samples. The peaks

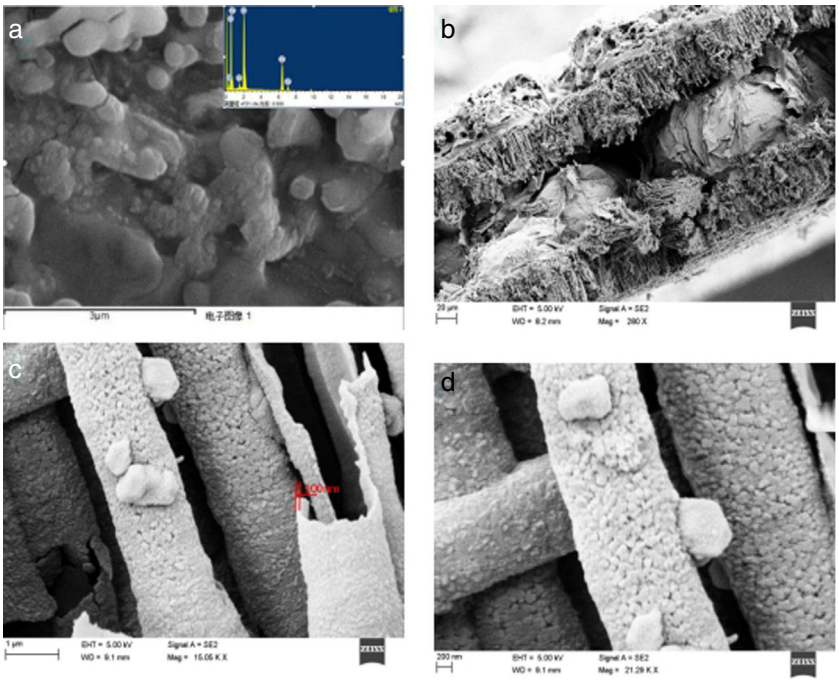

Fig. 3 – Scanning electron microscopy for the composite materials (a) surface composite materials in the aluminium foil (b) composite materials (c, d) tunnel structure enlargement in the tunnel of the aluminium foil section.

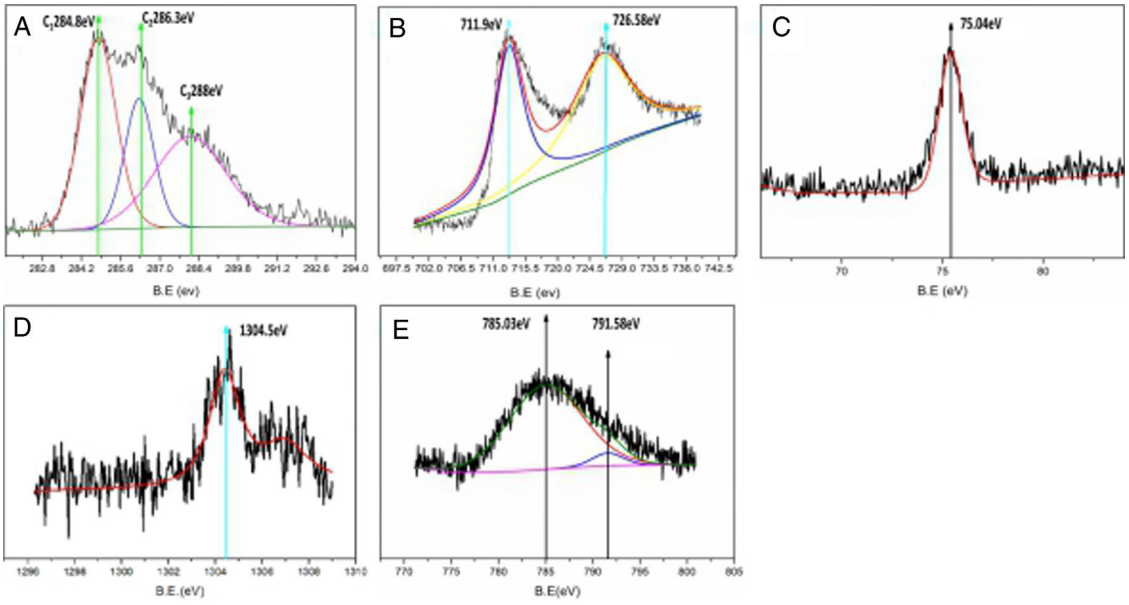

Fig. 4 – XPS elemental analysis of composites (A) Carbon, (B) Iron, (C) Aluminium, (D) Magnesium, (E) Cobalt.

at 711.9 eV and 726.58 eV correspond to Fe2p3/2 and Fe2p1/2, respectively. The binding energy is close to that of Fe(II). This shows that the iron element in the composite is divalent and that the reaction on the cathode aluminium foil (1) can occur. Compared with the traditional high-temperature solid-state process used for preparing lithium iron phosphate, the electrochemical deposition method directly prepared the trivalent ferrous into a bivalent ferrous, eliminating the process of carbon reduction. Increasing the uniformity of carbon for the in situ coating in electrodeposited composites is beneficial to improving the electrochemical properties of composites. The binding energy of the electron in Fig. 4C is 75.40 eV, corresponding to Al2p, which indicates that the Al element in the composites mainly exists in the form of Al^{3+}. Fig. 4D shows the energy spectrum analysis of the composite prepared by adding magnesium nitrate into the electrolyte during electrodeposition. The electron binding energy 1304.5 eV corresponds to the orbital binding energy of Mg1S. It shows that magnesium elements are doped into the composite in the form of divalent ions. Fig. 4E shows the energy spectrum analysis of the composite prepared by adding cobalt nitrate into the electrolyte during electrodeposition. The electron binding energies are

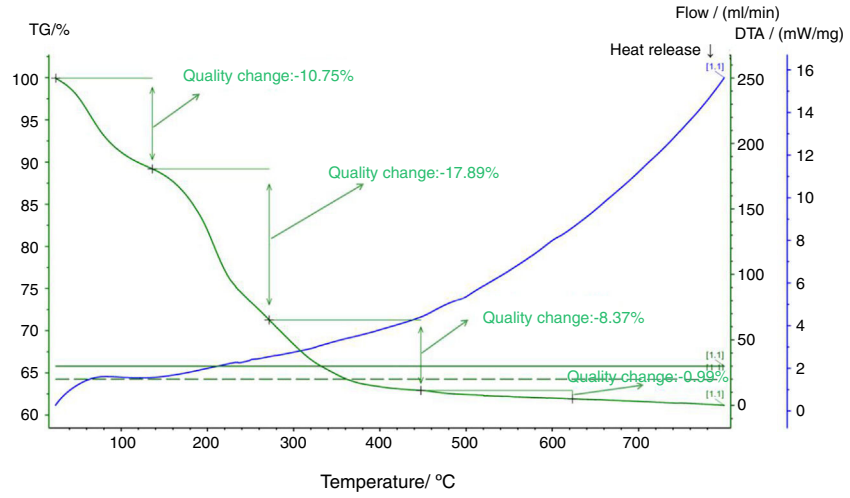

Fig. 5 – Composite thermal analysis diagram.

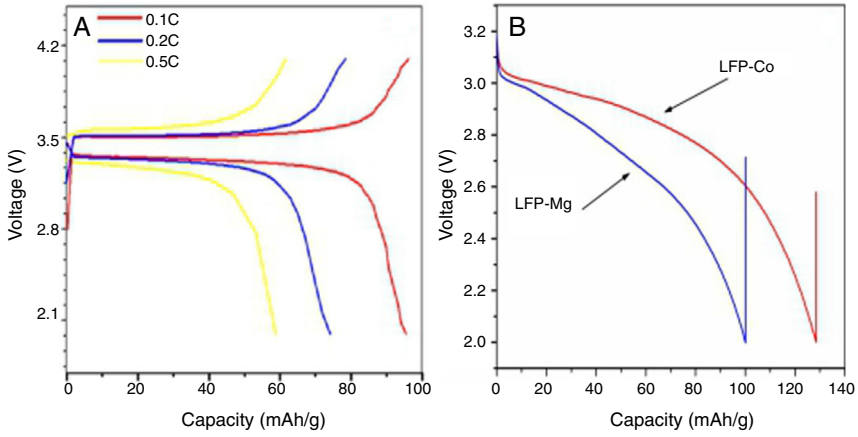

Fig. 6 – Battery charge and discharge test results (A: unmodified sample charge and discharge capacity at different rates; B: doped-modified sample at a 0.1 C rate discharge capacity).

791.58 eV and 785.03 eV. Corresponding to the orbital binding energy of Co 2p 3/2, this shows that cobalt elements are doped into the composites in the form of divalent ions. The results show that metal ions can be effectively doped into composite materials by adding metal ions into the electrolyte during electrodeposition. Lithium iron phosphate is an orthorhombic olivine structure in which tetrahedral PO_4 is located between octahedral FeO_6 layers, and Li in the intermediate structure is difficult to pass, thereby limiting its diffusion. In addition, FeO_6 is connected by a common apex, which has a large bond to the electrons in the outer layer of Fe, resulting in poor electronic conductivity. By adding the metal ions of the same valence state to replace the position of the ferrous ions in the original lattice, the original chemical bond changes, and the crystal structure is destroyed to a certain extent, which facilitates the passage of lithium ions, improves the conductivity, and reduces the impedance. This is beneficial to improve the electrochemical properties of the materials.

Fig. 5 shows a thermal analysis diagram of the composite precursor. Fig. 5 shows that the weight loss of the sample is 10.75% at 120 °C, which is mainly due to the content of free water in the precursor of the electrodeposited composites. The weightlessness between 120 °C and 260 °C is 17.89%, which is mainly caused by the carbonization of the organic matter in the precursor of the composite materials. The weightlessness between 260 °C and 440 °C is 8.37%, which is mainly caused by the formation of polyanion $Li_9Al_3P_8O_{29}$. According to the carbon element content in the organic matter, the carbon content in the composites is approximately 7%.

Electrochemical performance analysis

Fig. 6 shows a charge-discharge diagram measured by a battery test system after the composite materials were assembled into button batteries. Fig. 6A shows that the flat charging and discharging voltage platforms for batteries fabricated with the composite cathode occur at approximately 3.5 V and 3.4 V, respectively. This indicates that the deintercalation process for lithium ions in the lithium iron phosphate and the oxidation and reduction of Fe^{3+} and Fe^{2+} is stable. Under the condition of 0.1 C, the specific discharge capacity of the prepared sample is 95 mAh/g, the discharge capacity is 75 mAh/g at 0.2 C, and the discharge capacity is 59 mAh/g at 0.5 C. With an increase in the ratio, the capacity

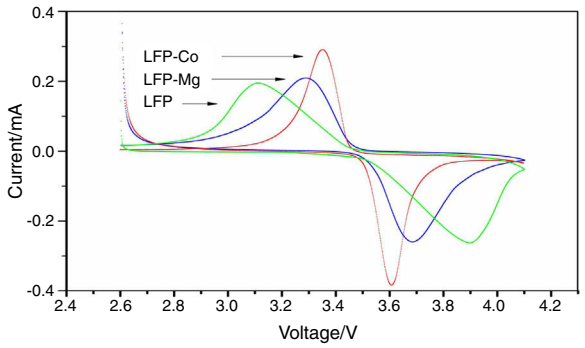

Fig. 7 – Cyclic voltammogram analysis results.

of the battery decreases gradually. Fig. 6B shows the specific capacity of the sample modified by doped metal ions at a 0.1 C rate after the first discharge. The specific capacities of the component LFP-Mg doped with magnesium ions and the component LFP-Co doped with cobalt ions are 100 mAh/g and 130 mAh/g, respectively. Compared with the sample without doping modification, the battery capacity is improved.

Compared with other researchers, the electrochemical properties of lithium iron phosphate prepared by electrochemical deposition still show some gaps. The main reason for the remaining gaps is that the polyanion in the composite materials affects the performance of the battery materials. In addition, the uniformity and content control of the carbon elements in the composite materials need to be further optimized to improve the electrochemical properties of the composite materials.

The cyclic voltammetric test results for composite materials assembled into button batteries are shown in Fig. 7. The graph shows that there are symmetrical redox peaks in the CV curve, which indicates that lithium ions are embedded and removed between the electrodes. The ratio of the redox peak to redox peak is close to 1, which reflects the reversibility of the electrode reaction. The above test results show that the prepared composite material has good stability. However, the results from cyclic voltammetry analysis before and after doping show that the shape of the peak for LFP-Mg is more symmetrical than that for LFP. In addition, the peak current increases and the difference between the oxidation potential and reduction potential decreases. This shows that the modified-doped Mg^{2+} can improve the reversibility of the battery and the cyclic performance of the battery. Comparing LFP-Co with the LFP-Mg composites, the difference in the redox peak potential was further increased by Co^{2+} doping, the peak current was further increased, and the symmetry between the redox peaks was further strengthened, which indicated that the polarization degree of the battery was smaller, and the electrical performance of the battery was further improved.

Fig. 8 shows the AC impedance test chart obtained after the composite materials were assembled into batteries. The frequency for the test spectrum ranged from 0.01 Hz to 100 kHz, and the amplitude was 5 mV. The dynamic reaction process for lithium -ion removal and embedding during the charging and discharging of the lithium-ion batteries was studied by electrochemical impedance spectroscopy (EIS) under the equilibrium potential condition. In the discharge state for lithium-ion batteries, the process of Li^+ embedment into cathode materials can be divided into four steps: first, Li^+ migrate from the electrolyte to the surface of the electrode material, followed by migration into the surface film. Then, charge transfer occurs in the boundary between the surface film and the cathode material. Finally, Li^+ diffuses from the surface of the cathode material towards the interior of the material. The charging process for lithium-ion batteries is the reverse of the discharge process. The curve in Fig. 8 is composed of a semicircular arc in the high-frequency region of load-transfer control and a straight line in the low-frequency region of diffusion control. The charge transfer resistance between the electrolyte and the electrode and the diffusion resistance for lithium ions in the charge-discharge process correspond to each other. Thus, they can be represented by equivalent circuit diagrams. In Fig. 8, Rs is the solution resistance, which shows the impedance for Li^+ migration in the electrolyte. CPE stands for double-layer capacitor. Rct is a charge transfer impedance, which indicates the charge transfer impedance for Li ions at the interface between the surface film and $LiFePO_4$ material. The impedance for lithium-ion diffusion from the surface to the inside of the lithium iron phosphate material is Zw.

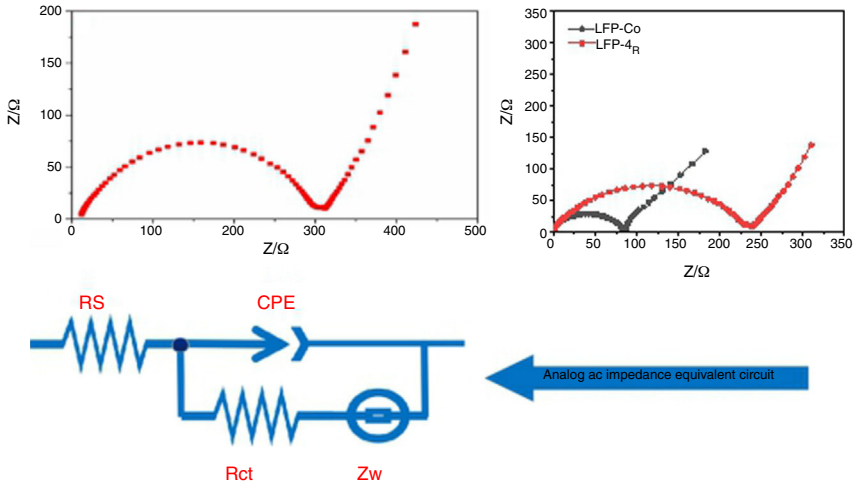

Fig. 8 – AC impedance test (A) un-modified. (B) Metal-ion doping modification treatment.

From the range of the semicircular arc in Fig. 8(A) and (B), it can be seen that the charge transfer resistance of the unmodified LFP and the modified LFP-Co and LFP-Mg in the high-frequency region is 300 Ω, 100 Ωand 250 Ω, respectively. The impedance for the doped cobalt ions in the high-frequency region is smaller than that for the unmodified samples and-doped magnesium ions. $LiFePO_4$ has an orthorhombic olivine structure. The tetrahedral PO_4 is located between the FeO_6 layers of the octahedron, and Li in the central position finds it difficult to pass through, which limits Li diffusion. In addition, FeO_6 is connected by common vertices, which greatly binds the electrons in the outer layer of Fe and makes the electron conductivity worse. Now, by adding metal ions with the same valence state to replace the position of the ferrous ions in the original lattice, the original chemical bonds are changed, and the crystal structure is destroyed to some extent, which is conducive to the passage of lithium ions, an improvement in the conductivity and a reduction of the impedance. The radius of Fe^{2+} is 0.061 nm. The radii of Mg^{2+} and Co^{2+} are 0.072 nm and 0.065 nm. Mg^{2+} and Co^{2+} replace the position of ferric ions in the original lattice, which changes the original chemical bond and facilitates the embedding and Embedding of lithium ions, respectively. When the same concentration of nitrate is added to the electrolyte, the lattice defects in lithium iron phosphate caused by cobalt ions enable Li^+ to be more easily embedded and desorbed.

Conclusions

In this paper, nanosized hollow aluminium matrix composites were prepared by electrodeposition using high purity aluminium foil cathode with a tunnel structure, graphite as anode, and a mixture of iron nitrate, lithium nitrate, phosphoric acid, glucose and CTAB as electrolyte in a propylene carbonate organic solvent. The results show that the composite is composed of olivine $LiFePO_4$ and polyanion $Li_9Al_3P_8O_{29}$. The particle size of the composite material on the surface of the aluminium foil ranges between 100 and 200 nm, and the composite material in the tunnel of the aluminium foil takes the form of a one-dimensional nano tube, with a particle size of 100 nm. After doping with Co^{2+}, the cell capacity increased from 95 mAh/g to 130 mAh/g at a rate of 0.1 C. The results from cyclic voltammetry and AC impedance analysis show that metal-ion doping improves the cyclic performance of the battery. In this paper, the battery material is prepared on the surface of Aluminium collector, which simplifies the installation process of lithium-ion battery and has good practical effect.

REFERENCES

[1] Y. Liu, J. Liu, J. Wang, et al., Formation of size-dependent and conductive phase on lithium iron phosphate during carbon coating, Nat. Commun. 9 (1.) (2018).

[2] T. Tsuda, N. Ando, T. Tanabe, et al., Improvement of high rate performance of a lithium ion battery composed of laminated $LiFePO_4$ cathodes/graphite anodes with porous electrode structure fabricated with a pico-second pulsed laser, Electrochim. Acta 291 (2018) 267–277.

[3] A. Milev, L. George, S. Khan, et al., Li-ion kinetics in $LiFePO_4$/carbon nanocomposite prepared by a two-step process: the role of phase composition, Electrochim. Acta 209 (2016) 565–573.

[4] I. Kim, P.A.R.K. Jinsoo, et al., Electrochemical properties of an as-deposited $LiFePO_4$ thin film electrode prepared by aerosol deposition, J. Power Sources 244 (Complete) (2013) 646–651.

[5] Z. Chen, M. Xu, B. Du, et al., Morphology control of lithium iron phosphate nanoparticles by soluble starch-assisted hydrothermal synthesis, J. Power Sources 272 (1) (2014) 837–844.

[6] P. Benedek, N. Wenzler, M. Yarema, et al., Low temperature hydrothermal synthesis of battery grade lithium iron phosphate, RSC Adv. 7 (29) (2017) 17763–17767.

[7] C. Rossouw, H. Zheng, K. Raju, et al., Microwave-assisted synthesis of graphene-coated Mn-doped lithium iron phosphate (LFMP/G) for electrochemical capacitor, J. Power Sources (2015).

[8] C.T. Hsieh, J.R. Liu, R.S. Juang, et al., Microwave synthesis of copper network onto lithium iron phosphate cathode materials for improved electrochemical performance, Mater. Chem. Phys. 153 (2015) 103–109.

[9] Y. Zhou, J. Lu, C. Deng, et al., Nitrogen-doped graphene guided formation of monodisperse microspheres of $LiFePO_4$ nanoplates as the positive electrode material of lithium-ion batteries, J. Mater. Chem. A (2016) 4.

[10] S. Yang, M. Hu, L. Xi, et al., Solvothermal synthesis of monodisperse $LiFePO_4$ micro hollow spheres as high performance cathode material for lithium ion batteries, ACS Appl. Mater. Interfaces 5 (18) (2013) 8961–8967.

[11] J. Tu, K. Wu, H. Tang, et al., Mg-Ti co-doping behavior of porous $LiFePO_4$ microspheres for high-rate lithium-ion batteries, J. Mater. Chem. A (2017), http://dx.doi.org/10.1039/C7TA04426G.

[12] I.D. Scott, Y.S. Jung, A.S. Cavanagh, et al., Ultrathin coatings on nano-$LiCoO_2$ for Li-ion vehicular applications, Nano Lett. 11 (2) (2011) 414–418.

[13] S. Luo, K. Wang, J. Wang, et al., ChemInform abstract: binder-free $LiCoO_2$/carbon nanotube cathodes for high-performance lithium ion batteries, Adv. Mater. 43 (30.) (2012).

[14] G. Saat, F.M. Balci, E.P. Alsaç, et al., Molten salt assisted self-assembly: synthesis of mesoporous $LiCoO_2$ and $LiMn_2O_4$ thin films and investigation of electrocatalytic water oxidation performance of lithium cobaltate, Small 14 (1.) (2018).

[15] Z. Quan, S. Ohguchi, M. Kawase, et al., Preparation of nanocrystalline $LiMn_2O_4$ thin film by electrodeposition method and its electrochemical performance for lithium battery, J. Power Sources 244 (Complete) (2013) 375–381.

[16] H. Zhang, H. Ning, J. Busbee, et al., Electroplating lithium transition metal oxides, Sci. Adv. 3 (5) (2017) e1602427.

[17] R. Xiao, K. Yan, Tunnel morphology of aluminum foil etched by a two-step DC etching method, Corros. Sci. 50 (11) (2008) 3256–3260, 11.